Numerical Study of Vortex Dynamics in Dipolar Bose Atomic Gases

Qiang Zhao[a,*], Hong-Jing Bi[b],

Xiao-Meng Yang[a] and Li-Li Zhang[c]

[a]*Department of Applied Physics, North China University of Science and Technology, Tangshan 063210, China*
[b]*Department of Computer Science, Tangshan Normal University, Tangshan 063000, China*
[c]*Center for Publishing, North China University of Science and Technology, Tangshan 063210, China*

In this paper, we study the dynamics of a single vortex and a corotating vortex pair in dipolar Bose–Einstein condensates under rotation. The results are obtained by numerically solving the nonlinear Gross–Pitaevskii equation. It is displayed that the dynamics behaviour is strongly dependent on the polarization angle and the rotation frequency. For a single vortex, the clockwise rotation occurs with an increasing rotation frequency, and the rotation direction is constant. The x coordinate and y coordinate as a function of time show that the single vortex is accelerated. The oscillation frequency is larger in the case of the totally repulsive dipolar interaction than for the anisotropic dipolar interaction. For a corotating vortex pair, the dynamic is different than in the case of a single vortex. When the rotation frequency is gradually increased, the corotating vortex pair spins from anti-clockwise to clockwise direction and the anisotropic dipolar interaction is fully embodied. In this process, the system has a critical rotation frequency to accomplish such transition. In addition, the vortex motion is confined to a small extent at this critical rotation frequency. These results reflect a competition between rotation and dipolar interaction.

topics: vortex motion, dipole–dipole interaction, Bose–Einstein condensates

1. Introduction

Quantized vortices, known as topological vortices, are a type of topological defect that can be stable in two dimensions (2D) as well as three dimensions (3D). Vortices in scalar [1, 2] and spinor [3–5], Bose–Einstein condensates (BECs) have been realized experimentally, providing a good platform to study the properties of the ground state and its dynamics. A lot of interesting physics is observed in the context of quantized vortices, for instance the rotating of superfluid He [6], interface physics of defect [7, 8], quantum turbulence [9–11] and vortex in droplet [12, 13] etc. For a review of the properties of vortices in BECs, please see [14, 15].

Among the many types of quantized vortices physics, low-number vortices such as a single vortex (SV) and two vortex with winding number of one and two, respectively, are an interesting and significant subject. The topic of small number vortices has been extensively investigated in the past few years. Gertjerenken et al. [16] studied the generation and manipulation on-demand of single vortex and two vortex, as well as the case of several vortices in a highly oblate atomic BECs in order to initialize complex vortex distributions for the study of vortex dynamics [16]. The role of the breathing width degree of freedom in the effective theory for the interacting two vortex systems in a trapped BEC under strong repulsive cubic nonlinearity was investigated [17]. It was found the rapid radial breathing oscillations superposed on the slower rotational motion of the vortex cores, which is justified by numerical solutions of the Gross–Pitaevskii (GP) equation. In [18], the authors expounded the dynamics of massive point vortices in a binary mixture of BECs. They showed that a massless single vortex with a rigid circular boundary can only precess uniformly. In addition, the two vortex precession and nutation dynamics of nonlinearly coupled, non-coaxial three-dimensional matter wave vortices were elaborated [19].

Dipole–dipole interaction (DDI) has been actively studied regardless of these topics, for example, low-lying collective excitation [20, 21], spin domain [22, 23], and tilted dipoles [24, 25]. In experiments, the orienting field [26] and the Feshbach resonance technique [27] enable us to tune the dipole strength and dipole scattering length, respectively. Moreover, because of the rich phenomena

generated by DDI, it is relatively effective to perform a theoretical analysis by using the GP model. In the work [28], it is demonstrated that the magnetic DDI can lead to observable effects in alkali-metal atom ^{87}Rb, the magnetic dipole moment of which is an order of magnitude lower than the ^{52}Cr atom.

In this work, we study the vortex dynamics of SV and a corotating vortex pair (CVP) in BEC when rotation is considered by performing extensive numerical calculations for a SV and CVP with long-range interactions. The CVP is a typical example of a two vortex model. In this case, it is natural to ask how the adding of a rotation modifies the dynamics of the vortex. Our results show that the dynamics behaviour presents different characteristics for SV and CVP. First of all for a SV, with increasing rotation frequency, clockwise rotation appears, and the rotation direction remains constant. In addition, $x(t)$ and $y(t)$ display that the single vortex is accelerated. The oscillation frequency for completely repulsive DDI is larger than for anisotropic DDI. Second, for a CVP, there is the critical rotation frequency Ω_c. In the case of rotation frequency when $\Omega < \Omega_c$ and $\Omega > \Omega_c$, the CVP rotates in an anti-clockwise and clockwise direction. Moreover, the anisotropic DDI is sufficiently reflected with increasing rotation frequency. At this critical point Ω_c, the vortex motion is confined to a small range. These results reflect the competition relationship between rotation and DDI.

The layout of this paper is as follows. In Sect. 2, we construct the theoretical model for 3D BECs, beginning from a mean-field theory, and giving a brief introduction to the numerical method. We present the main results of the paper in Sect. 3. We show the effect of the polarization angle and the rotation frequency on the dynamics behaviour of SV and CVP, and explain the physical cause found above. Finally, Sect. 4 is devoted to concluding remarks.

2. Theoretical model

We consider the dipolar BEC of N particles with mass m. At sufficiently low temperatures, the ground state of the condensate is well described by the time-dependent GP equation with the nonlocal DDI term [29, 30]

$$i\hbar\frac{\partial\phi(\boldsymbol{r},t)}{\partial t} = \Big[-\frac{\hbar^2}{2m}\nabla^2 + V(\boldsymbol{r})$$

$$-\Omega L_z + \frac{4\pi\hbar^2 a_s N}{m}|\phi(\boldsymbol{r},t)|^2$$

$$+N\int d\boldsymbol{r}'\, U_{dd}(\boldsymbol{r}-\boldsymbol{r}')\,|\phi(\boldsymbol{r}',t)|^2\Big]\phi(\boldsymbol{r},t), \quad (1)$$

where $V(\boldsymbol{r}) = \frac{m}{2}\big[\omega_\perp^2(x^2+y^2)+\omega_z^2 z^2\big]$ is the trap potential, $\omega_\perp$ and ω_z are the trap frequencies in the x–y plane and the z axis, respectively, and a_s is the atomic s-wave scattering length. The dipolar interaction is denoted

by $U_{dd}(\boldsymbol{R}) = \frac{\mu_0 g_F^2 \mu_B^2}{4\pi}(1-3\cos^2(\theta))/|\boldsymbol{R}|^3$ with the vacuum magnetic permeability μ_0, the Bohr magneton μ_B, and the Landé g-factor denoted by g_F. Here, $\boldsymbol{R} = \boldsymbol{r}-\boldsymbol{r}'$ is the relative position of dipoles and θ is the angle between the polarization axis $\boldsymbol{n}$ and $\boldsymbol{R}$ (i.e., $\cos(\theta) = \boldsymbol{n}\cdot\boldsymbol{R}/|\boldsymbol{R}|$). In (1), $L_z = i\hbar(y\partial x - x\partial y)$ is the z component of the orbital angular momentum operator and Ω is the rotation frequency. The macroscopic wave function is normalize to one, $\int d\boldsymbol{r}\, |\phi(\boldsymbol{r},t)|^2 = 1$.

It is convenient to use the GP equation in a dimensionless form. For simplicity, we make the transformation of variables as $\bar{\boldsymbol{r}} = \boldsymbol{r}/a_\perp$, $\bar{\boldsymbol{R}} = \boldsymbol{R}/a_\perp$, $\bar{t} = t\omega_\perp$, $\bar{\phi} = a_\perp^{3/2}\phi$, $\bar{\Omega} = \Omega\omega_\perp^{-1}$, $a_\perp = \sqrt{\hbar/(m\omega_\perp)}$. Thus, (1) can be expressed as

$$i\frac{\partial\phi(\boldsymbol{r},t)}{\partial t} = \Big[-\frac{1}{2}\nabla^2 + V(\boldsymbol{r})$$

$$+\frac{4\pi a_s N}{a_\perp}|\phi(\boldsymbol{r},t)|^2 - \Omega L_z + \frac{3Na_{dd}}{a_\perp}$$

$$\times \int d\boldsymbol{r}'\,\frac{(1-3\cos^2(\theta))}{|\boldsymbol{R}|^3}|\phi(\boldsymbol{r}',t)|^2\Big]\phi(\boldsymbol{r},t), \quad (2)$$

where $V(\boldsymbol{r}) = \frac{1}{2}(x^2+y^2+\lambda^2 z^2)$, $\lambda = \omega_z/\omega_\perp$, and $a_{dd} = \mu_0 g_F^2 \mu_B^2 m/(12\pi\hbar^2)$ is the dipole length scale. Next, scaled variables are shown without overhead bar, except if mentioned otherwise.

For an axially-symmetric pancake-shaped dipolar BEC with a strong axial trap ($\lambda > 1$), we assume that the dynamics in the axial direction is frozen. The wave function is written as

$$\phi(\boldsymbol{r},t) = f(z)\,\psi(\boldsymbol{\rho},t) = \frac{\exp\left(-\frac{z^2}{2d_z^2}\right)}{(\pi d_z^2)^{1/4}}\psi(\boldsymbol{\rho},t) \quad (3)$$

with $f(z)$ being the harmonic oscillator ground state along the axial direction, and $d_z = 1/\sqrt{\lambda}$. After integrating along the axial coordinate, a 2D dimensionless GP equation is obtained

$$i\frac{\partial\psi(\boldsymbol{\rho},t)}{\partial t} = \Big[-\frac{1}{2}\nabla_\rho^2 + V(\boldsymbol{\rho}) - \Omega L_z$$

$$+g|\psi(\boldsymbol{\rho},t)|^2 + g_d\Phi_{2D}\Big]\psi(\boldsymbol{\rho},t), \quad (4)$$

$$\Phi_{2D} = -\left(\partial_{\boldsymbol{n}_\perp \boldsymbol{n}_\perp} - n_3^2\nabla^2\right)$$

$$\times \int d\boldsymbol{\rho}'\, U_{2D}(\boldsymbol{\rho}-\boldsymbol{\rho}')\,|\psi(\boldsymbol{\rho}',t)|^2. \quad (5)$$

where

$$g = \frac{4\pi N}{\sqrt{2\pi}a_\perp}\left[\frac{a_s}{d_z} - \frac{a_{dd}}{d_z}(1-3n_3^2)\right], \quad (6)$$

$$g_d = \frac{m\mu_0 g_F^2 \mu_B^2 N}{2a_\perp\hbar^2}. \quad (7)$$

The term Φ_{2D} is a dipole integral with $\partial_{\boldsymbol{n}_\perp} = n_1\partial_x + n_2\partial_y$ and $\partial_{\boldsymbol{n}_\perp \boldsymbol{n}_\perp} = \partial_{\boldsymbol{n}_\perp}(\partial_{\boldsymbol{n}_\perp})$. The kernel U_{2D} is radially symmetric and is given by $U_{2D}(r) = \frac{1}{(2\pi)^{3/2}\sqrt{\lambda}}\exp(\frac{r^2}{4\lambda})K_0(\frac{r^2}{4\lambda})$, where K_ν denotes a modified Bessel function of the second kind (ν real) and $r^2 = (x-x')^2+(y-y')^2$. In (4)–(5), the dimensionless units $\hbar\omega_\perp$ is adopted for energy.
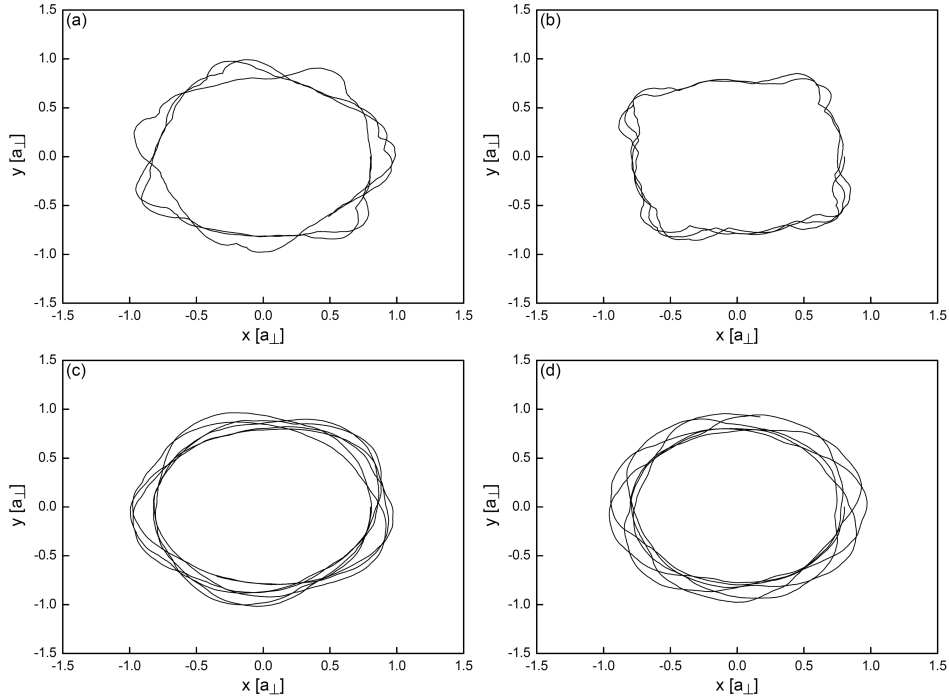
Fig. 1. Trajectory traversed by a SV for four different polarization angles and rotational frequencies. (a) $\alpha = 0$, $\Omega = 0.5\omega_\perp$ (b) $\alpha = \pi/2$, $\Omega = 0.5\omega_\perp$ (c) $\alpha = 0$, $\Omega = 0.7\omega_\perp$ (d) $\alpha = \pi/2$, $\Omega = 0.7\omega_\perp$. Simulation parameters: $a_{\mathrm{dd}}/a_s = 0.1$.

For the numerical calculations, the ground state wavefuction is prepared by imaginary time propagation Backward–Euler pseudospectral method [31], and dynamics is obtained by a second-order Strang time-splitting approach [32]. In addition, the dipolar integral is computed using convolution theorem with fast Fourier transform [33]. The space and time step is $\Delta x = \Delta y = 0.08$ and $\Delta t = 0.001$, respectively.

3. Results and discussion

In this manuscript, we consider $N \approx 6600$ atoms ^{52}Cr in a harmonic trap potential with $\omega_\perp = 2\pi \times 10$ Hz and $\omega_z = 2\pi \times 100$ Hz. The Landé g-factor of ^{52}Cr is $g_F = 6$ [64]. Natural dimensionless parameter $a_{\mathrm{dd}}/a_s = 0.1$ is used to characterize the relative strength of DDI and the s-wave contact interaction. In experiments, a_{dd} and a_s can be tuned by the magnetic Feshbach resonance technique. In what follows, we will discuss the dynamics of SV first, and then the CVP dynamics. According to the experimental study, the dipolar BEC is prepared in an oblate trap with magnetic dipoles oriented along the short direction of the trap. Therefore, in order to generate a SV in the system located at (x_1, y_1), where $x_1 = 0.8a_\perp$, $y_1 = 0$, we solve (4)–(5) in imaginary time with the DDI term Φ_{2D} and in the absence of the rotation term ΩL_z. After each step in the imaginary time evolution, we imprint the phase singularities corresponding to the presence of the vortex, i.e., the transformation

$$\Phi(t + \Delta t) = |\Phi| \exp\left(i\left[\tan^{-1}\left(\frac{y - y_1}{x - x_1}\right)\right]\right). \tag{8}$$

is performed. This solution is then substituted into in real time using (4)–(5) again, with the inclusion of the rotation term. Throughout this article, the tunable parameters are the rotation frequency Ω and the polarization angle α.

Figure 1 tracks the trajectory of SV at different polarization angles and rotation frequencies up to 100 s. In addition, we also plot the x coordinate and y coordinate of the vortex as a function of time, as shown in Fig. 2. The black solid line and the red dotted line represent the numerical results for $\alpha = 0$ and $\alpha = \pi/2$, respectively. One can see that the vortex with our initial position travels clockwise around the condensate in a direction. We analyze the effect of the slow rotation of $\Omega = 0.5\omega_\perp$ and the isotropic repulsive interaction $\alpha = 0$. In Fig. 1a, we observe that the trajectory twines with the development of time and a nonperiodic pattern is formed. Such behaviour is similar to the case of vortex dynamics without rotation and weak DDI [35]. Note that the vortex monotonously spirals out of the condensate as seen in [36, 37]. Increasing the polarization angle to $\alpha = \pi/2$ in Fig. 1b, the vortex behaviour is qualitatively in agreement with Fig. 1a, where the anisotropic DDI becomes dominant. For the dynamic evolution of the x coordinate (Fig. 2a) and the y coordinate (Fig. 2b), the oscillation frequency is larger for the repulsive interaction $\alpha = 0$ than for the anisotropic DDI $\alpha = \pi/2$.
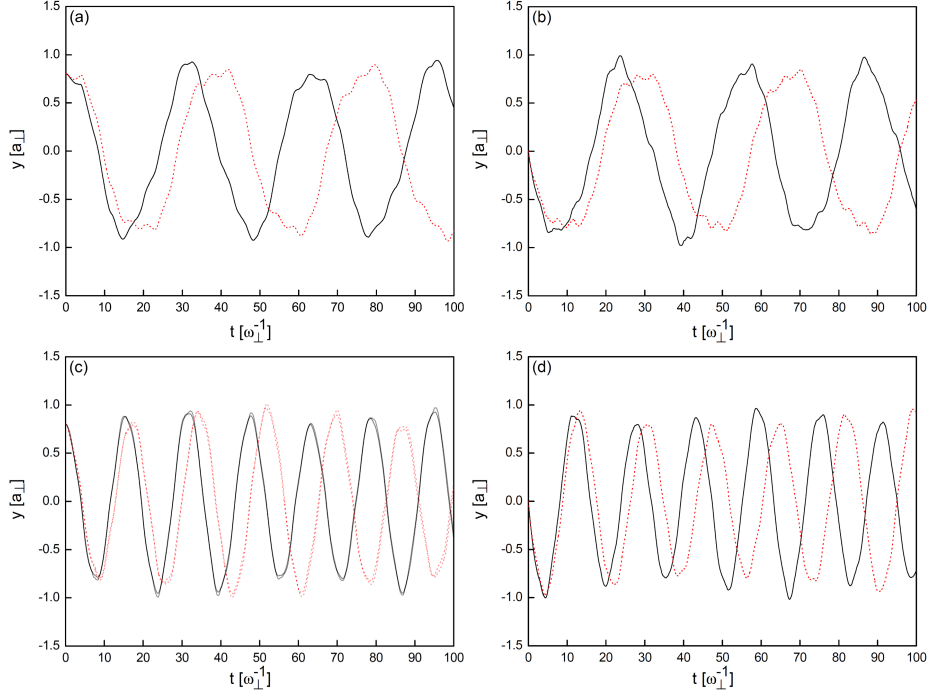
Fig. 2. The x and y coordinate of a SV as a function of time t for different rotational frequencies: (a, b) $\Omega = 0.5\omega_\perp$, (c, d) $\Omega = 0.7\omega_\perp$. The black solid line and red dotted line represent the numerical results for $\alpha = 0$ and $\alpha = \pi/2$, respectively. Simulation parameters: $a_{\mathrm{dd}}/a_s = 0.1$.

The reason for this difference is that the repulsive interaction between dipolar atoms accelerates the vortex motion, and the anisotropic DDI makes the movement of the vortex slower.

When the rotation frequency is increased to $\Omega = 0.7\omega_\perp$, the tangle behaviour of trajectory is still kept (Fig. 1c and d). The vortex coordinates x and y with respect to time are approaching the shape of the cosine wave, and their respective amplitudes in Fig. 1c and d are basically the same as in Fig. 1a and b. Moreover, it is evident that the vortex moves more and more fast. This is due to the fact that the direction of motion of a single vortex and a rotating trap is consistent. As a result, the increasing rotation frequency leads to an increase in the speed of vortex motion. Therefore, the period of $x(t)$ and $y(t)$ in Fig. 2c and d is smaller than in Fig. 2a and b. We confirmed that the direction of rotation of a SV keeps clockwise when the rotation frequency Ω is increased to the limit of the radial trap oscillator frequency $\omega_\perp$.

As discussed in previous part, we investigate the dynamics behaviour of CVP. First, we obtain the ground state by imaginary time, without rotation. Then we transform the wavefunction after each time step as follows

$$\Phi(t + \Delta t) = |\Phi| \exp \left\{ i \left[\tan^{-1} \left(\frac{y - y_1}{x - x_1} \right) \right. \right.$$

$$\left. \left. + \tan^{-1} \left(\frac{y - y_2}{x - x_2} \right) \right] \right\}. \tag{9}$$

Here $x_1 = 0.8a_\perp$, $y_1 = 0$ and $x_2 = -0.8a_\perp$, $y_2 = 0$ are the initial positions. This is to ensure that both vortices have the same radius and that they are opposite to each other in respect to the centre of the condensate. For convenience and illustrative purposes, a vortex with an initial location (x_1, y_1) and (x_2, y_2) is called as vortex 1 and vortex 2, respectively. It is evident that the two vortices rotate in a common direction due to the same spin. This point is an embodied form of (9). The solution created by this approach is shown in Figs. 3–5. It can be shown that, unlike in the above case, the vortex dynamics behaviour is more complicated.

Using the same method of tracking as we did before, when the condensate is rotated, for instance, $\Omega = 0.5\omega_\perp$, we observe that the two vortices spin about the centre in an anti-clockwise direction, which is different from the case of a SV. Figure 3a, b and Fig. 3c, d display the x coordinate and the y coordinate as a function of time for $\alpha = 0$ and $\alpha = \pi/2$. The black solid line and red dotted line correspond to vortex 1 and vortex 2, respectively. The $x(t)$ and $y(t)$ behaviour present rapidly oscillation, and it is seen that the oscillation frequency in $\alpha = \pi/2$ is almost same as for $\alpha = 0$. Nevertheless, the rapid oscillation significantly decreases as the rotation frequency increases to the critical value $\Omega_c = 0.65\omega_\perp$, as shown in Fig. 4. It is seen that the periodic motion of $x(t)$ and $y(t)$ is broken.

The facts imply that the vortex motion becomes slow, and thus vortex 1 and vortex 2 are confined in a small space extent. More importantly,
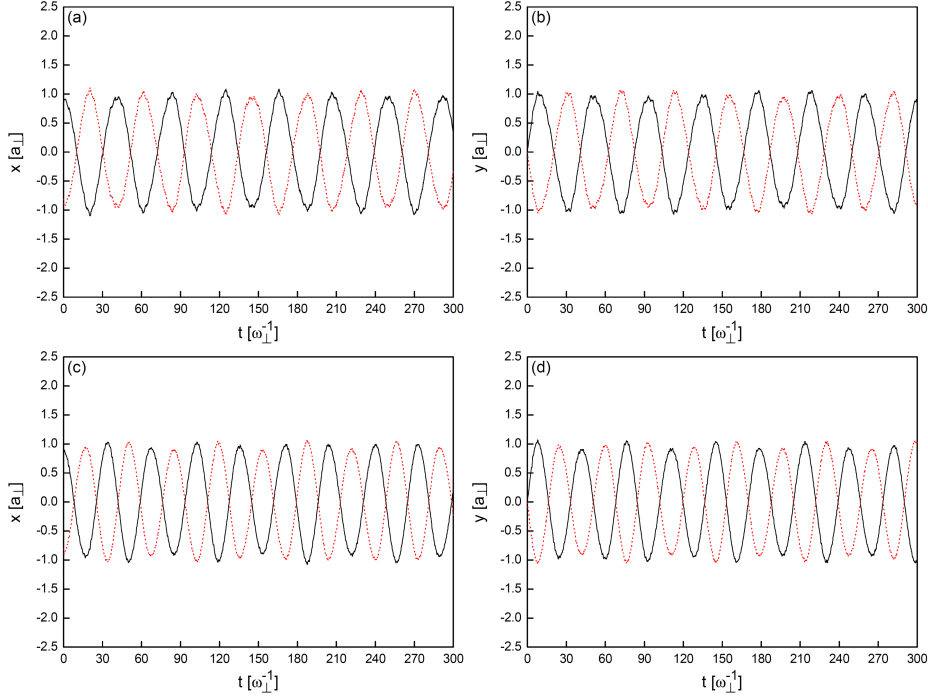
Fig. 3. The x and y coordinates of the vortices as a function of time t for different polarization angles and rotational frequencies: (a, b) $\alpha = 0$, $\Omega = 0.5\omega_\perp$, (c, d) $\alpha = \pi/2$, $\Omega = 0.5\omega_\perp$. The black solid line and red dotted line correspond to a CVP, respectively. Simulation parameters: $a_{\mathrm{dd}}/a_s = 0.1$.
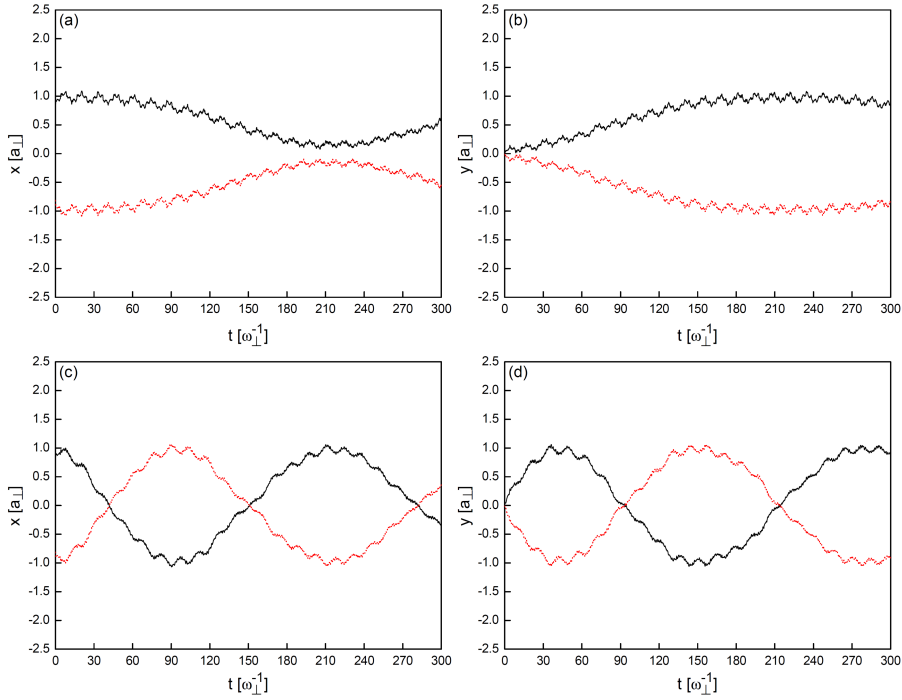

Fig. 4. Description as in Fig. 3 but for (a, b) $\alpha = 0$, $\Omega_c = 0.65\omega_\perp$, (c, d) $\alpha = \pi/2$, $\Omega_c = 0.65\omega_\perp$.

the anti-clockwise rotation is effectively weakened. As the rotation frequency is further increased to a larger value $\Omega = 0.8\omega_\perp$ (see Fig. 5), the CVP rotate clockwise about the centre, and the periodicity of $x(t)$ and $y(t)$ recovers. The oscillation frequency in $\alpha = \pi/2$ is smaller than the case of $\alpha = 0$. This phenomenon is consistent with the observation in Fig. 2 and shows that the effects of DDI on the vortex motion are fully embodied. As a consequence, we can see that the CVP turns back
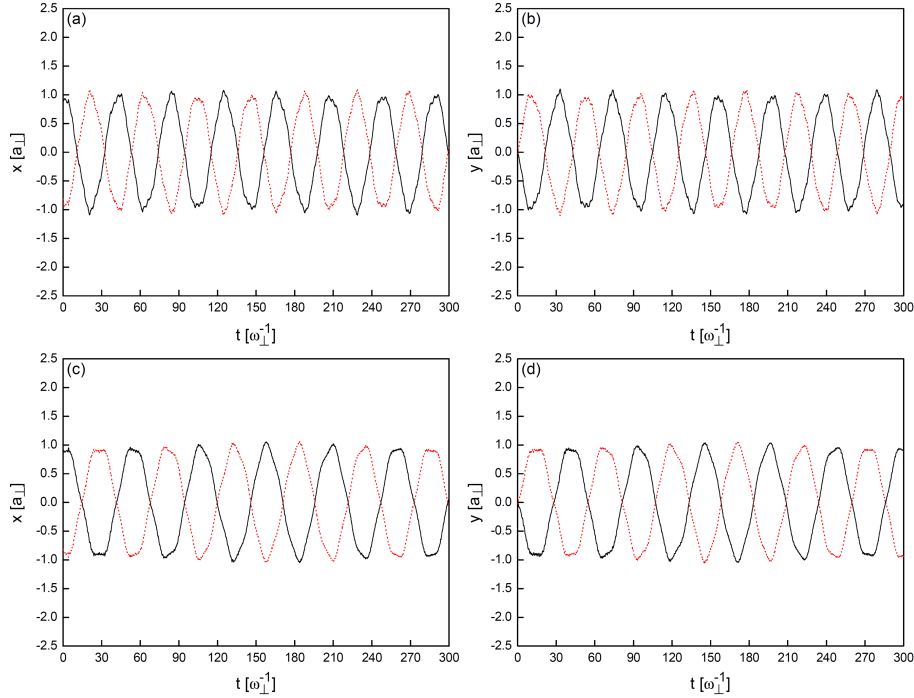
Fig. 5. Description as in Fig. 3 but for (a, b) $\alpha = 0$, $\Omega = 0.8\omega_\perp$, (c, d) $\alpha = \pi/2$, $\Omega = 0.8\omega_\perp$.

with the increase of rotation frequency. This behaviour of the vortex motion is not observed in the previous study and it is completely different than in the case of a single vortex, where the direction of the motion of a single vortex keeps clockwise about the centre, regardless of the value of the rotation frequency.

4. Conclusions

In conclusion, we investigate the vortex dynamics for a single and a corotating vortex pair in rotating dipolar BECs. We show how dynamic behaviour depends on the polarization angle and the rotation frequency. For a SV, it rotates in a clockwise direction as the rotation frequency increases, while the rotation direction keeps unchange. The x coordinate and y coordinate as a function of time show that a SV speeds up and thus the oscillation frequency becomes large. In addition, the oscillation frequencies of $x(t)$ and $y(t)$ for $\alpha = 0$ are greater than for $\alpha = \pi/2$. This is due to the DDI being purely repulsive in the former and anisotropic in the latter. From the physical point of view, the repulsive and anisotropic DDI respectively accelerate and decelerate the vortex motion. On the other hand, the CVP shows distinct dynamics behaviour as the rotation frequency increases. When the rotation frequency is small, the CVP spins in an anti-clockwise direction and the oscillation frequency of $x(t)$ and $y(t)$ for $\alpha = \pi/2$ is almost the same as for $\alpha = 0$. On the contrary, a clockwise rotation is observed when the rotation frequency exceeds a critical value and the oscillation frequency of $x(t)$ and $y(t)$ is smaller than

for $\alpha = 0$. In this process, the anisotropic dipolar interaction is thoroughly expressed. Moreover, the vortex motion of the CVP is limited to a small extent at the critical rotation frequency. These facts reflect the competition relationship between rotation and DDI.

References

[1] T. Mithun, K. Porsezian, B. Dey, *Phys. Rev. A* **89**, 053625 (2014).

[2] R. Driben, V.V. Konotop, B.A. Malomed, T. Meier, *Phys. Rev. E* **94**, 012207 (2016).

[3] L.A. Williamson, P.B. Blakie, *Phys. Rev. A* **94**, 063615 (2016).

[4] L.A. Williamson, P.B. Blakie, *Phys. Rev. Res.* **3**, 013154 (2021).

[5] H. Zhu, C.F. Liu, D.S. Wang, S.G. Yin, L. Zhuang, W.M. Liu, *Phys. Rev. A* **104**, 053325 (2021).

[6] R.J. Donnelly, *J. Fluid Mech.* **233**, 691 (1991).

[7] M.O. Borgh, J. Ruostekoski, *Phys. Rev. A* **87**, 033617 (2013).

[8] M.O. Borgh, J. Ruostekoski, *Phys. Rev. Lett.* **109**, 015302 (2012).

[9] A. Cidrim, A.C. White, A.J. Allen, V.S. Bagnato, C.F. Barenghi, *Phys. Rev. A* **96**, 023617 (2017).

[10] P.C. di Leoni, P.D. Mininni, M.E. Brachet, *Phys. Rev. A* **92**, 063632 (2015).

[11] T.P. Billam, M.T. Reeves, A.S. Bradley, *Phys. Rev. A* **91**, 023615 (2015).

[12] M. Nilsson Tengstrand, P. Stürmer, E.Ö. Karabulut, S. M. Reimann, *Phys. Rev. Lett.* **123**, 160405 (2019).

[13] M. Pi, F. Ancilotto, J.M. Escartín, R. Mayol, M. Barranco, *Phys. Rev. B* **102**, 060502(R) (2020).

[14] A.L. Fetter, *Rev. Mod. Phys.* **81**, 647 (2009).

[15] M. Tsubota, K. Kasamatsu, M. Kobayashi, in: *Novel Superfluids*, Vol. 1, Oxford University Press, Oxford 2013.

[16] B. Gertjerenken, P. G. Kevrekidis, R. Carretero-González, B.P. Anderson, *Phys. Rev. A* **93**, 023604 (2016).

[17] K. Nakamura, D. Babajanov, D. Matrasulov, M. Kobayashi, P. Muruganandam, *J. Phys. A* **49**, 315102 (2016).

[18] A. Richaud, V. Penna, A.L. Fetter, *Phys. Rev. A* **103**, 023311 (2021).

[19] R. Driben, V.V. Konotop, T. Meier, *Sci. Rep.* **6**, 22758 (2016).

[20] L.J. Jia, A.B. Wang, S. Yi, *Phys. Rev. A* **97**, 043614 (2018).

[21] S. X. Deng, T. Shi, S. Yi, *Phys. Rev. A* **102**, 013305 (2020).

[22] T. Świsłocki, T. Sowiński, J. Pietraszewicz, M. Brewczyk, M. Lewenstein, J. Zakrzewski, M. Gajda, *Phys. Rev. A* **83**, 063617 (2011).

[23] R.M. Wilson, B.M. Anderson, C.W. Clark, *Phys. Rev. Lett.* **111**, 185303 (2013).

[24] H.K. Wu, W.L. Tu, *Phys. Rev. A* **102**, 053306 (2020).

[25] S.B. Prasad, B.C. Mulkerin, A.M. Martin, *Phys. Rev. A* **103**, 033322 (2021).

[26] S. Giovanazzi, A. Görlitz, T. Pfau, *Phys. Rev. Lett.* **89**, 130401 (2002).

[27] C. Chin, R. Grimm, P. Julienne, E. Tiesinga, *Rev. Mod. Phys.* **82**, 1225 (2010).

[28] M. Vengalattore, S.R. Leslie, J. Guzman, D.M. Stamper-Kurn, *Phys. Rev. Lett.* **100**, 170403 (2008).

[29] Y.Y. Cai, M. Rosenkranz, Z. Lei, W.Z. Bao, *Phys. Rev. A* **82**, 043623 (2010).

[30] Y.Y. Cai, Y.J. Yuan, M. Rosenkranz, H. Pu, W.Z. Bao, *Phys. Rev. A* **98**, 023610 (2018).

[31] W.Z. Bao, I.L. Chern, F.Y. Lim, *J. Comput. Phys.* **217**, 612 (2006).

[32] H.Q. Wang, W.Z. Bao, *J. Comput. Phys.* **187**, 318 (2006).

[33] W.Z. Bao, Y.Y. Cai, H.Q. Wang, *J. Comput. Phys.* **229**, 7874 (2010).

[34] A. Griesmaier, J. Werner, S. Hensler, J. Stuhler, T. Pfau, *Phys. Rev. Lett.* **94**, 160401 (2005).

[35] Q. Zhao, *J. Low Temp. Phys.* **204**, 1 (2021).

[36] S. Gautam, A. Roy, S. Mukerjee, *Phys. Rev. A* **89**, 013612 (2014).

[37] S. Gautam, *J. Phys. B* **47**, 165301 (2014).